

Simulations of cementite: An analytical potential for the Fe-C system

K. O. E. Henriksson^{1,*} and K. Nordlund²

¹*Department of Reactor Physics, Royal Institute of Technology, S-10691 Stockholm, Sweden*

²*Department of Physics, University of Helsinki, P.O. Box 43, FI-00014 University of Helsinki, Finland*

(Received 15 February 2009; published 6 April 2009)

An analytical bond-order interatomic potential has been developed for the iron-carbon system for use in molecular-dynamics and Monte Carlo simulations. The potential has been successfully fitted to cementite and Hägg carbide, which are most important crystalline polytypes among the many known metastable iron carbide phases. Predicted properties of other carbides and the simplest point defects are in good to reasonable agreement with available data from experiments and density-functional theory calculations. The potential correctly describes melting and recrystallization of cementite, making it useful for simulation of steels. We show that they correctly describe the metastability of cementite and can be used to model carbide growth and dissolution.

DOI: [10.1103/PhysRevB.79.144107](https://doi.org/10.1103/PhysRevB.79.144107)

PACS number(s): 81.05.Je, 71.15.Nc, 71.15.Pd, 77.84.Bw

Ferrous alloys, and especially steels, are abundant in modern-day society due to cheap availability of Fe and the large versatility of the finished product. The main carbide constituent of model steels such as Fe-C alloys is cementite Fe_3C , which occurs in the form of lamellae or small precipitates.^{1,2} Depending on the C content, the microstructure may be ferrite, austenite, and martensite—with C occurring as interstitial atoms—or the more complicated pearlite, bainite, and spheroidite. All these phases basically consist of ferrite and cementite Fe_3C . The study and design of new steels—for instance in nuclear applications—are therefore dependent on a good description of cementite, with power to predict mechanical and thermal effects. Molecular-dynamics (MD) and Monte Carlo (MC) simulations are among the cheapest methods to investigate this type of effects with atomistic detail. However, these techniques require accurate interatomic potentials. To date, only one of the most recent Fe-C potentials³⁻⁵ seems to be able to handle cementite. According to Lau *et al.*³ their parametrization gives reasonable formation energies of C-related defects as well as cementite. However, proper elastic properties and behavior at elevated temperatures or under irradiation were not verified. A successful potential should not only get most properties of cementite right, but also at least the Hägg carbide Fe_5C_2 ,^{6,7} since the former is known to occur as a precursor to cementite.^{6,8}

The analytical bond-order potential (ABOP) formalism (see Ref. 9 and references therein) is a suitable approach for a potential that is able to describe different bonding types. It is essentially a modified form of the Brenner^{10,11} and Tersoff¹² potentials, which were originally developed for C-H and Si, respectively. The ABOP formalism has been used previously for metals, semiconductors, and combinations of these, such as Ga-As,⁹ Si-C,¹³ and Pt-C.¹⁴ In this paper we present such a potential for the Fe-C system. The current parameterization describes the cementite, Hägg, and Eckstrom-Adcock (Fe_7C_3) carbides, the melting and recrystallization of cementite, as well as some point defect systems.

Most details of the present calculations of physical properties—such as formation energy, bulk modulus, and elastic constants—can be found in Ref. 15. For the binding energy of a defect configuration $A_1 + \dots + A_n$, where A_i may

be a C atom or a vacancy, we used¹⁶ $E_b(A_1 + \dots + A_n) = \sum_i E(A_i) - E(A_1 + \dots + A_n) - (n-1)E_{\text{ref}}$, where $E(A_i)$ is the energy of the cell containing only defect A_i , $E(A_1 + \dots + A_n)$ is the energy of the cell containing the composite defect, and E_{ref} is the energy of the cell without any defects. The structures used for fitting were taken from our previous density-functional theory (DFT) calculations of Fe and Cr carbides.¹⁵ The fitting database included the Fe-C dimer, the simple CsCl, NaCl (rocksalt), and ZnS (zinc-blende) phases, as well as cementite and Hägg carbide. Point defect systems were not included. As mentioned above, the Hägg carbide occurs as a precursor for cementite in steels, so to ensure correct energetics both had to be considered. The testing database included the Eckstrom-Adcock carbide (originally found in catalysts used for hydrocarbon synthesis) and the somewhat theoretical carbide Fe_4C . The actual fitting was performed with the TULIP computer code.¹⁷

The properties of the fitted carbides are shown in Tables I and II. The potential is in good agreement with DFT and available experimental data for the carbides Fe_3C and Fe_5C_2 . Although the formation energies are somewhat underestimated, the relative ordering of (meta)stability is correct.

The potential parameterization is given in Table III. The Fe-Fe and C-C interactions have been taken from the literature. In the ABOP formalism the total potential energy is

$$V = \sum_{ij} V_{ij} = \frac{1}{2} \sum_{ij} f_c(r_{ij}) [V_R(r_{ij}) - b_{ij} V_A(r_{ij})],$$

where $f_c(r) = 1$ when $r \leq |R-D|$, $f_c(r) = 0$ when $r \geq |R+D|$, and

$$f_c(r) = \frac{1}{2} - \frac{1}{2} \sin\left(\frac{\pi}{2D}(r-R)\right)$$

otherwise. Here r_{ij} is the distance between atoms i and j . Atoms further apart than $R+D$ do not interact, i.e., this is the cutoff distance of the interaction. The Morse-type terms are

$$V_R(r) = \frac{D_0}{S-1} \exp[-\beta\sqrt{2S}(r-r_0)],$$

TABLE I. Experimental and density-functional theory (DFT) properties of Fe carbides used as fitting targets. a, b, c are the lattice parameters (unit: Å), r_0 is the bond length of the dimer (Å), E_f is the formation energy (or enthalpy) (eV) and is given for the molecule (not per unit cell or atom), D_0 is the bond energy for the dimer (eV), B is the bulk modulus (GPa), and $B'(P) \equiv \partial B / \partial P$ is the pressure derivative of the bulk modulus. First line: experimental data, second line: *ab initio* data, and third line: result predicted by the potential.

Structure (phase)	Property					
	a or r_0	b	c	E_f or D_0	B	$B'(P)$
Fe-C dimer	1.596 ^a			3.96 ^a		
	1.5962 ^b , 1.578 ^c			3.47 ^b , 3.89 ^c		
	1.514			2.369		
FeC (CsCl)	–			–	–	–
	2.467 ^d			1.87 ^d	343 ^d	4.4 ^d
	2.404			1.18	313	4.4
FeC (NaCl)	–			–	–	–
	3.92 ^e , 3.996 ^d			1.16 ^d	329 ^d	4.4 ^d
	3.916			1.49	273	4.4
FeC (ZnS)	–			–	–	–
	4.254 ^d			0.87 ^d	251 ^d	4.2 ^d
	4.104			1.67	202	4.2
Fe ₃ C	5.0787 ^f , 5.0896 ^g	6.7297 ^f , 6.7443 ^g	4.5144 ^f , 4.5248 ^g	0.23 ^h		
	5.024 ^d	6.754 ^d	4.478 ^d	0.22 ⁱ , 0.18 ^d	243 ^j , 234 ^d	4.0 ^d
	5.086	6.521	4.498	0.12	235	4.5
Fe ₅ C ₂	11.562 ^k , 11.588 ^l	4.5727 ^k , 4.579 ^l	5.0595 ^k , 5.059 ^l			
	11.504 ^m , 11.614 ^d	4.524 ^m , 4.507 ^d	5.012 ^m , 4.987 ^d	0.31 ^d	209 ^m , 252 ^d	5.2 ^d
	11.609	4.497	4.878	0.20	289	4.5

^aReference in Ref. 19.

^bReference 18.

^cReference 19.

^dReference 15.

^eReference 20.

^fReference 21.

^gReference 22.

^hReference 23.

ⁱReference 24.

^jReference 25.

^kReference 6.

^lReference 7.

^mReference 26.

$$V_A(r) = \frac{SD_0}{S-1} \exp[-\beta\sqrt{2/S}(r-r_0)].$$

$$g(\theta) = \gamma \left(1 + \frac{c^2}{d^2} - \frac{c^2}{d^2 + (h + \cos \theta)^2} \right).$$

The bond order is $b_{ij} = (1 + \chi_{ij})^{-1/2}$, where

$$\chi_{ij} = \sum_{k,k \neq i, k \neq j} f_c(r_{ik}) g_{ik}(\theta_{ijk}) \omega_{ijk} e^{\alpha_{ijk}(r_{ij}-r_{ik})},$$

For simulations of high-energy events—which occur in e.g., sputtering simulations—the energy expression for r close to 0 needs to be modified. A simple yet effective modified potential is

$$\tilde{V}_{ij} = F(r_{ij})V_{ij} + V_{ZBL}(r_{ij})[1 - F(r_{ij})],$$

TABLE II. DFT and fitted elastic constants of cementite Fe₃C all in units of GPa.

	C_{11}	C_{22}	C_{33}	C_{44}	C_{12}	C_{13}	C_{23}	C_{55}	C_{66}
DFT ^a	394	412	360	83	157	146	166	133	136
ABOP	363	406	388	91	181	166	130	125	134

^aReference 15.

TABLE III. The potential parameterizations used in the present work. The last column contains the presently developed potential. All $\alpha_{ijk}=0$ and $\omega_{ijk}=1$.

Parameter	Fe-Fe ^a	C-C ^b	Fe-C
D_0 (eV)	1.5	6.0	4.826 451 34
r_0 (Å)	2.29	1.39	1.477 365 10
β (Å ⁻¹)	1.4	2.1	1.632 081 70
S	2.0693109	1.22	1.431 347 55
γ	0.0115751	2.0813×10^{-4}	0.002 058 62
c	1.2898716	330.0	8.955 832 21
d	0.3413219	3.5	0.720 620 47
h	-0.26	1.0	0.870 998 74
R (Å)	3.15	1.85	2.5
D (Å)	0.2	0.15	0.2
r_f (Å)	0.95	0.6	1
b_f (Å ⁻¹)	2.9	8	10

^aReferences 28 and 29.

^bReferences 10 and 30.

where $V_{ZBL}(r)$ is the universal repulsive Ziegler-Biersack-Littmark potential,²⁷ $F(r)$ is the Fermi-Dirac function $F(r) = (1 + \exp[-b_f(r-r_f)])^{-1}$, and b_f and r_f are fitting parameters giving a smooth joined potential, such that the equilibrium properties of the original potential are maintained.

The potential was tested on the carbides Fe₇C₃ and Fe₄C, with fairly good predicted properties, most of them being less than 15% off (see Table IV). Only the formation energy of Fe₄C is problematic, being 60% too small. But it is still the largest one for all the real-world carbides (all those except the CsCl, NaCl, and ZnS phases). It should also be noted that Fe₄C has not actually been verified experimentally by independent researchers.

We also calculated the formation energies E_f for octahedral, tetrahedral, and substitutional C in body-centered-cubic (bcc) Fe. The energies are 1.18, 1.50, and 2.84, respectively, all in eV. DFT calculations¹⁶ give energies of 0.80, 1.70, and 3.16, respectively, all in eV. The present value for the octahedral site is higher than in DFT; the others are smaller but deviate by only $\approx 10\%$.

TABLE IV. Predicted properties of Fe carbides. See Table I for the legend.

Compound (phase)	Property					
	a	b	c	E_f	B	$B'(P)$
Fe ₇ C ₃	6.882 ^a ,4.540 ^b	6.882 ^a ,6.879 ^b	4.540 ^a ,11.942 ^b			
	4.517 ^c	6.866 ^c	11.743 ^c	0.54 ^c	262 ^c	3.7 ^c
	4.468	7.011	11.396	0.44	286	4.1
Fe ₄ C	3.878 ^d					
	3.751 ^e ,3.837 ^c			2.50 ^c	199 ^e ,173 ^c	4.6 ^c
	3.763			1.09	179	4.1

^aReference 31.

^bReference 32.

^cReference 15.

^dReference 33.

^eReference 34.

TABLE V. Binding energies (eV) of simple defect systems in Fe containing C atoms and vacancies (V). The DFT results are for cells with 128 lattice sites. In the MD simulations 1024 lattice sites were used.

System	DFT ^a	Present work
2 C, Fig. 1(a)		
Config. 1	-0.65	-0.46
Config. 2	-0.09	-0.10
Config. 3	-1.67	-0.77
Config. 4	-0.09	-0.10
Config. 5	0.13	0.13
Config. 6	0.14	-0.01
Config. 7	0.16	0.07
C+ vacancy, Fig. 1(b)		
Config. 1	0.47	0.21
Config. 2	-0.01	-0.03
Config. 3	-0.33 ^b	-0.10
Config. 4	-0.11 ^b	-0.33 ^c
C+(110), Fig. 1(c)		
Config. 1	-0.19	0.75
Config. 2	-0.31	0.07
Config. 3	-0.09	0.56

^aReference 16.

^bCalculated for a cell of 54 atoms.

^cNote: the relaxed position for the C atom is actually a slightly off-center configuration 3.

The potential has also been applied to more complicated point defects in bcc Fe. The initial configurations are illustrated in Fig. 1, and the binding energies E_b are given in Table V together with results from DFT calculations.¹⁶ The overall agreement is very good. The relaxed states are very close to the initial ones in the case if two octahedral C atoms [Fig. 1(a)]. In the case of a C atom interacting with a vacancy [Fig. 1(b)], there are some noticeable relaxations taking

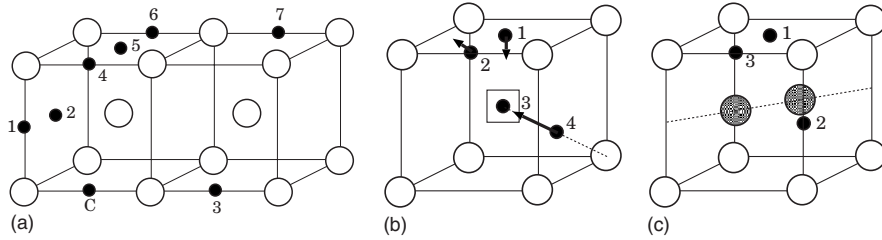


FIG. 1. Initial positions of (a) two C atoms in bcc Fe (each pair consists of the “C” atom and any of the other numbered C atoms); (b) one C atom and one vacancy in bcc Fe; and (c) one C atom and one $\langle 110 \rangle$ self-interstitial dumbbell in bcc Fe. Open circles represent Fe atoms, filled circles C atoms, open squares vacancies, and hatched circles the dumbbell. Black arrows indicate approximate relaxed C atom positions. C atom number 4 in (b) is initially halfway between the Fe corner atom and the vacancy, but relaxes to very close to the vacancy, only 0.23 \AA from it.

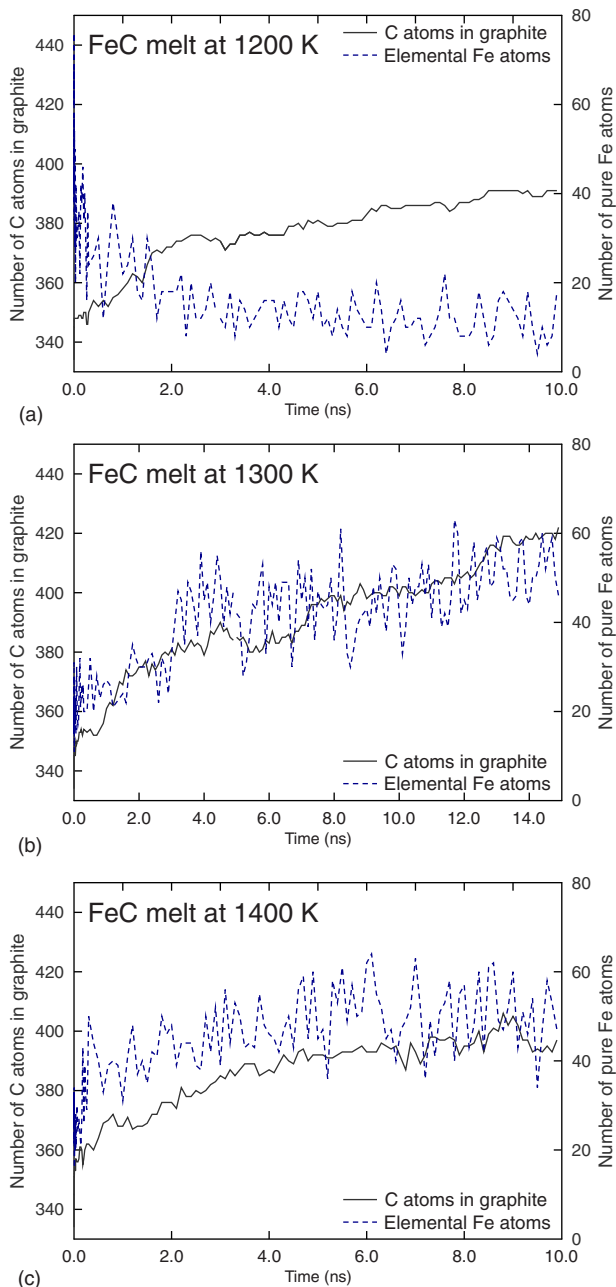


FIG. 2. (Color online) The number of C atoms in graphite and Fe atoms in fcc environment, as a function of time, at 1200, 1300, and 1400 K.

place. The most important one is for configuration 4, where the C atom initially halfway between the vacancy and a Fe corner atom, relaxes toward the vacancy, and ends up slightly off-center, about $0.24 \text{ \AA} \approx 0.05a_0$, where $a_0 = 2.889 \text{ \AA}$ is the relaxed lattice parameter, away from it, still in the $\langle 111 \rangle$ direction. In other words, the initial configuration 4 is completely unstable.

The most problematic E_b values have been obtained for the $\langle 110 \rangle$ self-interstitial (SIA) dumbbell interacting with a single C atom [see Fig. 1(c)]. DFT results indicate that all three mentioned configurations should be nonbinding, but the potential gives the opposite behavior. In addition, a closer look at the atomic relaxations shows that the local environment of the C atom is heavily distorted. In light of this, the present parameterization should be avoided for systems featuring interstitial C and SIA dumbbells.

The diffusion of a C atom in bcc Fe was simulated at temperatures between 600 and 1200 K, with the latter being roughly half of the melting temperature predicted by the potential.²⁹ The results fit well on an Arrhenius curve $D(T) = D_0 \exp[-E_m/(k_B T)]$, where $D_0 = (2.0 \pm 0.2) \times 10^{-8} \text{ m}^2 \text{ s}^{-1}$ is the diffusion prefactor, $E_m = 0.267 \pm 0.007 \text{ eV}$ the migration activation energy, k_B Boltzmann’s constant, and T the temperature. The prefactor and the activation energy are lower than the experimental values of $4.876 \times 10^{-7} \text{ m}^2 \text{ s}^{-1}$ and 0.8359 eV , respectively.³⁵

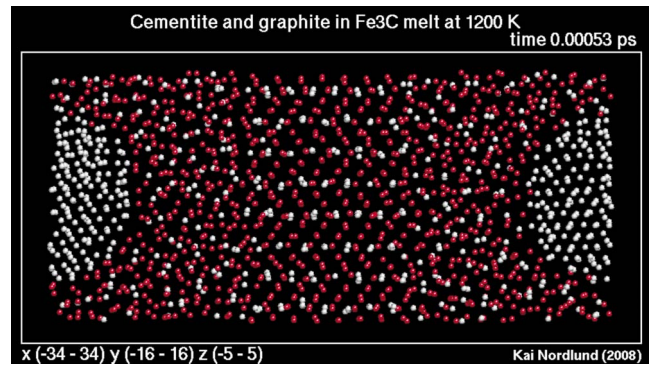
Since cementite is a metastable compound, it does not have a well-defined melting point. However, experimentally it is observed that cementite decomposes between 1100 and 1200 K.¹ To study the phase stability of cementite described by our interatomic potential, we created cells with a solid cementite and liquid Fe_3C in a bilayer structure, simulated it at various temperatures for time scales up to 1 ns, and monitored whether the solid or liquid phase grows. We found that up to temperatures of 1200 K, the solid phase grew, and at and above 1300 K, the whole cell melted. Considering that interatomic potentials often predict the melting points of even pure elements wrong by tens of percents, the agreement between the current simulated and experimental decomposition temperature ranges can be considered very good.

The decomposition above 1200 K can, based on the equilibrium Fe-C phase diagram,^{1,2} occur into austenite (fcc) Fe and graphite. Since it is difficult to nucleate graphite, we also made simulation cells with a solid cementite and liquid Fe_3C in a bilayer structure as well as a graphite inclusion inside the liquid part. These systems were simulated at 1200, 1300,

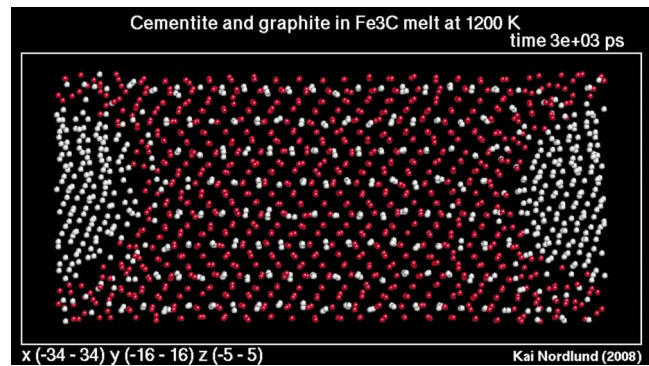
and 1400 K for time scales of 10–15 ns. Visual analysis showed that at 1300 K and above the cementite melted, as expected from the previous simulations without the graphite inclusion. However, the graphite did not melt, but steadily grew in size, and pure Fe also started to slowly form in the simulation cell (see Fig. 2). Analysis of the bonding environment of the pure Fe atoms showed that they had the austenite and not the ferrite structure. At 1400 K the behavior was similar, but due to the higher temperature, the fluctuations in the number of graphite or pure Fe atoms were higher and the long-term trend harder to distinguish.

At 1200 K the crystalline cementite grew at the expense of the liquid phase until the cementite and graphite crystalline phases covered the whole simulation cell. The situations are shown in Fig. 3, at 0 and 3 ns since start. After the recrystallization the graphite phase started to grow at the expense of the cementite. This is to be expected since cementite is metastable. The removal of C atoms from cementite leads to an associated removal of Fe atoms. Analysis showed that the number of bcc- or fcc-coordinated Fe atoms oscillated between 1 and 10, indicating that these are actually in a molten solution. It is evident from Fig. 3 that the parasitic growth of graphite is slow after the whole cell has crystallized at about 2–3 ns. If graphite continues to grow it is not unreasonable to expect cementite to continue to dissolve and austenite to eventually start forming. Extended simulations beyond current computer capacity limitations would be needed to prove this conclusively.

In summary, an analytical bond-order potential has been developed for the Fe-C system. The pure Fe part from the literature describes both austenite and ferrite as well as the Bain path. The full Fe-C potential gives a good description of the basic physical properties of cementite Fe_3C , Hägg carbide Fe_5C_2 , and Eckstrom-Adcock carbide Fe_7C_3 , as well as most of the point defect systems tested. In addition, the potential successfully describes the melting and recrystalli-



(a)



(b)

FIG. 3. (Color online) Snapshots of the FeC melt at 1200 K at (a) 0 ns and (b) 3 ns since start. White balls represent C atoms.

zation of cementite. These results indicate that the potential can be used to simulate steels.

K.O.E.H. acknowledges funding from the European Commission via Intra-European Foundation (Euratom) [Contract No. 036446 (FU06)].

*krister.henriksson@helsinki.fi

¹W. D. Callister, *Materials Science and Engineering*, 5th ed. (Wiley, New York, 2000).

²B. S. Mitchell, *An Introduction to Materials Engineering and Science: For Chemical and Materials Engineers* (Wiley, New York, 2008).

³T. T. Lau, C. J. Först, X. Lin, J. D. Gale, S. Yip, and K. J. VanVliet, *Phys. Rev. Lett.* **98**, 215501 (2007).

⁴C. Becquart, J. M. Raulot, G. Bencteux, C. Domain, M. Perez, S. Garruchet, and H. Nguyen, *Comput. Mater. Sci.* **40**, 119 (2007).

⁵D. J. Hepburn and G. J. Ackland, *Phys. Rev. B* **78**, 165115 (2008).

⁶K. H. Jack and S. Wild, *Nature (London)* **212**, 248 (1966).

⁷J. J. Retief, *Powder Diffr.* **14**, 130 (1999).

⁸S. Nagakura and S. Oketani, *J. Iron Steel Inst., London* **8**, 265 (1968).

⁹K. Albe, K. Nordlund, J. Nord, and A. Kuronen, *Phys. Rev. B* **66**, 035205 (2002).

¹⁰D. W. Brenner, *Phys. Rev. B* **42**, 9458 (1990).

¹¹D. W. Brenner, *Phys. Rev. B* **46**, 1948 (1992).

¹²J. Tersoff, *Phys. Rev. Lett.* **56**, 632 (1986).

¹³P. Erhart and K. Albe, *Phys. Rev. B* **71**, 035211 (2005).

¹⁴K. Albe, K. Nordlund, and R. S. Averback, *Phys. Rev. B* **65**, 195124 (2002).

¹⁵K. O. E. Henriksson, N. Sandberg, and J. Wallenius, *Appl. Phys. Lett.* **93**, 191912 (2008).

¹⁶C. Domain, C. S. Becquart, and J. Foct, *Phys. Rev. B* **69**, 144112 (2004).

¹⁷K. O. E. Henriksson, TULIP computer code, 2008.

¹⁸S. S. Itono, T. Taketsugu, T. Hirano, and U. Nagashima, *J. Chem. Phys.* **115**, 11213 (2001).

¹⁹D. Tzeli and A. Mavridis, *J. Chem. Phys.* **118**, 4984 (2003).

²⁰L. Cheng-Bin, L. Ming-Kai, Y. Dong, L. Fu-Qing, and F. Xiang-Jun, *Chin. Phys.* **14**, 2287 (2005).

²¹H. Lipson and N. J. Petch, *Trans. Iron Steel Inst. Jpn.* **142**, 95 (1940).

²²E. J. Fasiska and G. A. Jeffrey, *Acta Crystallogr.* **19**, 463 (1965).

²³M.-I. Lee and G. Simkovich, *Metall. Trans. A* **19**, 2115 (1988).

- ²⁴I. R. Shein, N. I. Medvedeva, and A. L. Ivanovskii, *Physica B* **371**, 126 (2006).
- ²⁵C. Jiang, S. G. Srinivasan, A. Caro, and S. A. Maloy, *J. Appl. Phys.* **103**, 043502 (2008).
- ²⁶H. I. Faraoun, Y. D. Zhang, C. Esling, and H. Aourag, *J. Appl. Phys.* **99**, 093508 (2006).
- ²⁷J. F. Ziegler, J. P. Biersack, and U. Littmark, *The Stopping and Range of Ions in Matter* (Pergamon, New York, 1985).
- ²⁸M. Müller, P. Erhart, and K. Albe, *J. Phys.: Condens. Matter* **19**, 326220 (2007).
- ²⁹C. Bjorkas and K. Nordlund, *Nucl. Instrum. Methods Phys. Res. B* **259**, 853 (2007).
- ³⁰N. Juslin, J. Nord, K. O. E. Henriksson, P. Traskelin, E. Salonen, K. Nordlund, P. Erhart, and K. Albe, *J. Appl. Phys.* **98**, 123520 (2005).
- ³¹F. H. Herbstein and J. A. Snyman, *Inorg. Chem.* **3**, 894 (1964).
- ³²R. Fruchart, J.-P. Sénateur, J.-P. Bouchaud, and A. Michel, *C. R. Hebd. Seances Acad. Sci.* **260**, 913 (1965).
- ³³P. Villars and L. D. Calvert, *Pearson's Handbook of Crystallographic Data for Intermetallic Phases* (American Society for Metals, Metals Park, OH, 1985).
- ³⁴A. V. dos Santos, M. I. da Costa, and C. A. Kuhnen, *J. Magn. Magn. Mater.* **166**, 223 (1997).
- ³⁵R. B. McLellan and M. L. Wasz, *J. Phys. Chem. Solids* **54**, 583 (1993).